Understanding Diffusion in Nanoporous Materials

E. Beerdsen,* D. Dubbeldam, and B. Smit

Van 't Hoff Institute for Molecular Sciences, University of Amsterdam, Nieuwe Achtergracht 166, 1018 WV Amsterdam, The Netherlands

Centre Européen de Calcul Atomique et Moleculaire (Cecam), Ecole Normale Supérieure, 46 Allée d'Italie, 69007 Lyon, France

(Received 12 October 2005; published 30 January 2006)

Can we predict diffusion behavior of molecules in confinement by looking at the match between the molecule and the structure of the confinement? This question has proven difficult to answer for many decades. As a case study, we use methane and a simple model of ellipsoids to arrive at a molecular picture that allows us to make a classification of pore topologies and to explain their diffusion behavior as a function of loading. Our model is surprisingly simple: regarding a structure as consisting of interconnected ellipsoids is enough to understand the full loading dependence.

DOI: 10.1103/PhysRevLett.96.044501 PACS numbers: 47.56.+r, 66.30.−h, 82.75.Jn

Membranes function because of differences in diffusion and adsorption of the molecules that are adsorbed in these materials. Many different materials are used as membranes. Lipid bilayers in cell membranes and molecular sieves such as zeolites in industrial separation are just a few examples. Common to these nanoporous materials is that they contain pores that have sizes similar to the dimensions of the adsorbed molecules and therefore impose a tight confinement. This makes the diffusion behavior of adsorbed molecules in these materials very much different from diffusion in a bulk fluid [1–10]. Well studied though these systems are, their diffusion properties remain poorly understood. In an elaborate study, comparing the diffusion of four gases in four zeolite topologies, Skoulidas and Sholl found widely varying diffusion trends, showing the potential of tuning diffusion for industrial processes by adjusting the loading [4,11]. Despite the importance for many applications, conventional methods, such as molecular dynamics (MD), cannot explain when and why, for a given system, the diffusion will increase, decrease, or remain constant as a function of loading.

In this work, we make use of a very simple model based on ellipsoids, to present a fundamental understanding of the loading dependence, and analyze the molecular factors causing the observed behavior.

There are many ways of expressing diffusion behavior in a diffusion coefficient. Macroscopic methods, like measurements of the uptake rate and permeation rate, typically yield the transport diffusion coefficient D_T. It is given by Fick's law: $J = -D_T \nabla c$, where J is the sorbate flux when a concentration gradient ∇c is applied. To obtain a diffusion coefficient that is presumably less dependent on loading [1], D_T is often converted to the corrected diffusivity D_C, also known as the Maxwell-Stefan or Darken diffusivity: $D_C = D_T \frac{\delta \ln c}{\delta \ln f}$ (with c the sorbent concentration or loading and f the fugacity). The self- or tracer-diffusion coefficient D_S, finally, is a quantity that can be obtained by microscopic methods, such as pulsed field gradient NMR (PFG NMR). It can be interpreted as the diffusion of a single tagged particle making its way through the porous medium and, if present, other particles. At the infinite dilution limit, D_S, D_C, and D_T are strictly equivalent. For reasons of convenience, the corrected diffusivity has been assumed to be relatively insensitive to changes in concentration. Although historically inaccurate, this is often referred to as the Darken approximation [9,12] and it has received widespread application [1]. It has been the basis for extrapolations to compare different data sets and relate microscopic and macroscopic diffusion processes. Although many deviations have been found, where the corrected diffusivity was concentration dependent, they were seen as exceptions on the general rule [4].

In this work we focus on the influence of the confinement on the various diffusion coefficients. Therefore, we use rigid siliceous molecular sieve structures, devoid of cations. Owing to their regular crystalline shapes and wide variety of topologies, they are ideal model systems [2–7,13–16].

We use a combination of conventional MD calculations and our recently proposed dynamically corrected transition state theory (dcTST) method [17–19]. In addition to diffusion coefficients, this method can yield an explanation of the diffusion behavior in terms of free-energy differences. Free-energy profiles are computed during an NVT-ensemble Monte Carlo (MC) or MD simulation, in which we compute the probability to find a particle at a particular value of the reaction coordinate q. Further details about the method can be found in Ref. [17].

Zeolites are designated by three-letter codes. D_S and D_C were obtained for methane in 10 different sieve topologies: LTA, CHA, ERI, SAS, AFI, MTW, LTL, MFI, BOG, and BEC; this set represents a wide range of different topologies (see Table I). We focused on methane, since even for this simple molecule the diffusion behavior is not understood. The results are shown in Fig. 1.

We can interpret our results by making use of a very simple concept based on ellipsoids. The molecular sieve's pores or cavities form confinements that can be thought of

TABLE I. Structural data for the ten examined structures. For each topology, the table lists the window ring size in number of oxygen atoms per ring, the window diameter, the cage diameter [Å] (perpendicular to the long axis a), and the cage-to-window ratio R_{ctw}. The cage and window data left and right for intersecting channel topologies are the values for the channels in the different directions. Where the window diameter is given as a range, this signifies that the windows have an oval shape. The values for R_{ctw} in these cases are calculated as the ratio of the smallest diameter of the oval to the diameter of the cage.

	Ring size	Window diameter [Å]	Cage diameter [Å]	Cage-to-window ratio R_{ctw}
LTA	8	4.1	10	2.44
ERI	8	3.6–5.1	11	3.06
CHA	8	3.8	8.5	2.24
SAS	8	4.2	10	2.38
LTL	12	7.1	13	1.83
MTW	12	5.6–6.0	8	1.42
AFI	12	7.3	10	1.37
BOG	12/10	7.0/5.5–5.8	···	···
ISV	12/12	6.1–6.5/5.9–6.6	···	···
MFI	10/10	5.1–5.5/5.3–5.6	···	···

as interconnected ellipsoids. There are three ways to interconnect these ellipsoids [see Fig. 2 (left)]: aligned in a direction perpendicular to the long axis a (top), aligned along a (middle), or aligned alternatingly (bottom). The three base models form confinement types that we refer to as "cage-type," "channel-type," and "intersecting channel-type," respectively, and each of these types gives rise to a very distinct diffusion behavior (see Fig. 1). The first and second model differ only in the direction in which the ellipsoids are connected. In fact, we can make a transition from a cagelike system (top) to a tubelike structure (middle) by changing the aspect ratio of the ellipsoids. However, the diffusion behavior is qualitatively different when the ellipsoids are connected along their long axis or along their short axis. Therefore, we see them as different classes. The left-hand side of Fig. 2 shows the way the ellipsoids are connected in each of the three models along with the predicted free-energy profiles. The right-hand side of the figure shows examples of sieve topologies from each class, together with the calculated free-energy profiles, strikingly similar to the schematic predictions.

The cage-type molecular sieves [Fig. 2 (top)] generally consist of large cages, connected by narrow windows forming large free-energy barriers. The molecules' inter-

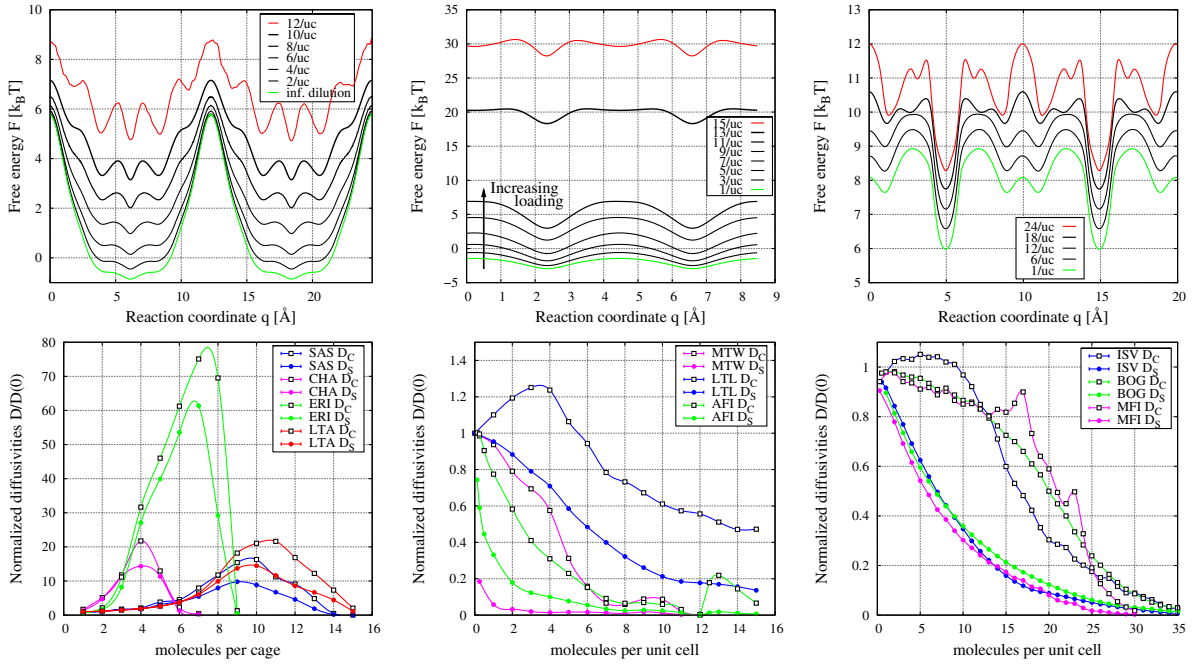

FIG. 1 (color online). (Top) Free-energy profiles as a function of loading for cage-type LTA (left), channel-type AFI (middle), and intersecting channel-type MFI (right), at 300 K (bottom). Normalized D_S and D_C as a function of loading for cage-type SAS, CHA, ERI, and LTA (left), channel-type MTW, LTL, and AFI (middle), and intersecting channel-type ISV, BOG, and MFI (right). Loadings are given in molecules/uc for (intersecting) channel-type structures, and in molecules/cage for cage-type structures.

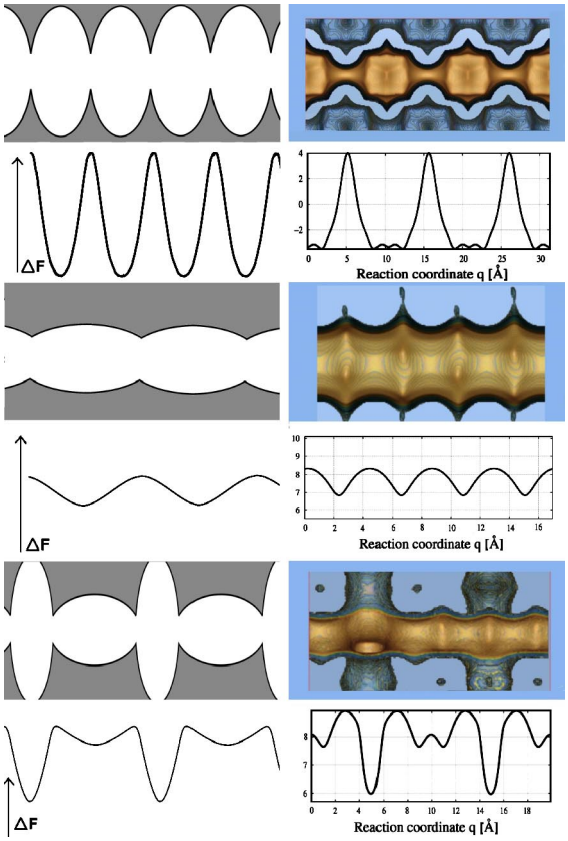

FIG. 2 (color online). (Left) Three ways to connect ellipsoids, (top) aligned in a direction perpendicular to the long axis a, (middle) aligned along a, (bottom) aligned alternatingly. Below each ellipsoidal model on the left, a schematic representation is given of the associated free-energy profile. (Right) Examples of molecular sieves that correspond to each of the ellipsoidal models: SAS (top), AFI (middle), and MFI (bottom), each with their calculated free-energy profile (zero loading); the true free-energy profiles are very similar to the schematic ones.

action with the sieve wall is favorable. With every molecule that is added to a cage, more of this interaction is being exchanged for less favorable interaction with other molecules [17], causing an increase in the free energy of the bottom of the well, as shown in Fig. 1 (top, left) for methane in LTA-type molecular sieve. The influence of particles at the window region is much smaller, so that as the structure is being filled up, the net free-energy barrier decreases, causing an *increase* in both the self- and the transport-diffusion coefficient. At very high density, packing and free-volume effects cause the emergence of new, smaller, free-energy barriers, inside the cages, in addition to those in the windows, causing the diffusion to decrease. In Fig. 1 (bottom, left) we show that LTA-, ERI-, CHA-, and SAS-type systems all conform to this scenario for the diffusion of methane. The increase in both self- and corrected-diffusion compared to the infinite dilution limit can be a surprising *two orders* of magnitude. As expected, $D_C > D_S$ in all cases, due to positively contributing correlations present in D_C, but not in D_S. Clearly, if we change the size of the cage the position of the maximum of the diffusion coefficient will change accordingly. This is exactly what we observe for SAS, LTA, ERI, and CHA. LTA and SAS have the same type of cages, the largest of the four topologies (based on the saturation loading), while CHA has the smallest.

The second class of confinement consists of channel-type molecular sieves [Fig. 2 (middle)]. Upon insertion of new molecules, again the free energy in the interior of the cage rises, but this time the effect on the free energy is even larger at the barriers [Fig. 1 (bottom, middle)]. As a result, the diffusivity (both D_S and D_C) is a decreasing function of loading [Fig. 1 (bottom, middle)]. The details of the diffusion graph depend on the exact topology of the channels. The smoother the channel (i.e., the wider the windows with respect to the cages, or the smaller R_{ctw}), the steeper the decreasing function will be. In channel-type structures, the amount of collective behavior is much higher than in cage-type structures, because the barriers are lower. The difference between D_S and D_c depends on the window size: the smaller the intersection between ellipsoids, the larger the ratio D_C/D_S. MTW has the narrowest windows and has the largest D_C/D_S. LTL, which consists of relatively wide cages interconnected by intermediate windows ($R_{\mathrm{ctw}} = 1.83$), can be considered as a transition between the truly cage-type and the smooth channel-type molecular sieves. Note the small peak in D_C for AFI at high loadings. At 12 molecules per unit cell, there is an optimal packing of molecules, which does not allow them to shift around much. Increasing the loading further requires a large increase in pressure (accordingly, there is an inflection in the adsorption isotherm), and forces the molecules to leave their optimum-packing positions (the number of molecules becomes incommensurate with the lattice). This causes a rise in the diffusion, peaking around 13 molecules per unit cell, upon which the molecules reorder according to a new optimum packing, allowing 15 molecules per unit cell.

The third class of confinement is the class of intersecting channel-type structures [Fig. 2 (bottom)], of which MFI is the most famous example. Any type of structure with channels running in different directions that mutually intersect falls into this category. The barriers are formed by the horizontally aligned ellipsoids, creating entropic traps between consecutive vertical ellipsoids. The influence of loading in these systems is complex as it involves effects such as unsimultaneous freezing in vertical and horizontal ellipsoids/channels, due to differences in ellipsoid diameter and length, causing varying degrees of commensurability of the particles with the structure, as a function of loading and direction. Here, like in the case of channel-type molecular sieves, the self-diffusion still sharply decreases when the loading is increased, but the corrected diffusivity initially only slightly decreases with density, until packing effects sharply decrease the corrected diffusivity to zero, causing a kink in the diffusion curve at intermediate loading [Fig. 1 (bottom, right)]. The position of the highest free-energy barrier is not the same for every

loading. Importantly, the corrected diffusion starts its fast decrease at the exact loading where the barrier which is highest at low loading is overtaken by a new barrier, giving rise to a new diffusion regime.

Note that for all scenarios, both D_S and D_C approach zero at the maximum loading, due to packing effects that halt the diffusion, irrespective of the topology of the confinement, in violation of the Darken approximation. This decrease of diffusion can be delayed to higher loading by free-energy effects: adsorbing molecules that lower the free-energy barrier have a favorable effect on the diffusion. The loading at which the final decrease sets in is determined by the size of the cage and the topology of the confinement. This observation implies that the Darken approximation generally cannot be used outside a very small region near zero loading [19].

We stress that the ordering of molecular sieve structures in classes depends strictly on the combination of adsorbate and adsorbent. The method employed in this study can be used to make a classification of pore structures for any given adsorbate molecule. It turns out that for methane the border between cage-type and channel-type structures lies at an R_{ctw} of around 2. For larger molecules, such as benzene, this border is likely to shift towards lower values of R_{ctw}. When applying this classification to larger molecules, sieve structures can therefore ''switch class,'' but the general behavior will be the same: when the cages are large (with respect to the adsorbed molecule) and the windows are narrow, the diffusion as a function of loading will go through a maximum; when the confinement is experienced as a smooth channel, the diffusion is a decreasing function of loading [this has also been observed for small alkanes in carbon nanotubes [20]]; when the confinement consists of intersecting channels, D_S will be monotonously decreasing as a function of loading, and D_C will show a kink. At high loadings in MFI, the diffusion becomes increasingly dominated by secondary corrugation. A better description of the diffusivity as a function of loading would require a higher-order model, consisting of ellipsoids of different types. In a recent Letter, we have shown that the erratic diffusion graph of MFI can be fully explained by the free-energy profiles [19].

It would be instructive to compare our simulation results with experimental data. A detailed comparison, however, requires experimental transport and self-diffusion coefficients for a large range of loadings. At present, such sets of experimental data are not available. Experimentally, it is difficult to measure diffusion over a large range of loadings. Different methods often result in diffusion coefficients that can differ orders of magnitude from one another [1]. Only recently an experimental technique became available to measure D_S and D_C simultaneously [6]. Chong *et al.* have performed self- and collective-diffusion measurements of ethane in MFI, using one single experimental technique over the entire loading range [21]. It is encouraging that for the systems where experimental data have been obtained, namely, ethane in MFI, the agreement between simulation and experiment is good. This gives some confidence that the classification gives a correct prediction for the examined all-silica versions of the structures. Our classification methodology may also help the interpretation of those experimental data that are often limited to a narrow (loading) window.

We thank R. Krishna and H. Jobic for stimulating discussions, the Netherlands Research Council (CW), and the Deutsche Forschungsgemeinschaft (DFG, priority program SPP 1155) for financial support, and NWO/NCF for computational resources.

*Corresponding author.
Email address: beerdsen@science.uva.nl.

[1] J. Kaerger and D. M. Ruthven, *Diffusion in Zeolites and Other Microporous Solids* (Wiley, New York, 1992).
[2] E. J. Maginn, A. T. Bell, and D. N. Theodorou, J. Phys. Chem. **100**, 7155 (1996).
[3] R. Q. Snurr, A. T. Bell, and D. N. Theodorou, J. Phys. Chem. **98**, 11 948 (1994).
[4] A. Skoulidas and D. S. Sholl, J. Phys. Chem. A **107**, 10 132 (2003).
[5] S. M. Auerbach, Int. Rev. Phys. Chem. **19**, 155 (2000).
[6] H. Jobic, J. Karger, and M. Bee, Phys. Rev. Lett. **82**, 4260 (1999).
[7] S. Fritzsche, M. Gaub, R. Haberlandt, and G. Hofmann, J. Mol. Model. **2**, 286 (1996).
[8] R. Krishna, J. M. van Baten, and D. Dubbeldam, J. Phys. Chem. B **108**, 14 820 (2004).
[9] H. Ramanan and S. M. Auerbach, in ''NATO-ASI Series C: Fluid Transport in Nanopores,'' edited by J. Fraissard and W. Conner (Kluwer Academic Publishers, Dordrecht, to be published).
[10] J. Xiao and J. Wei, Chem. Eng. Sci. **47**, 1123 (1992).
[11] A. I. Skoulidas, D. S. Sholl, and R. Krishna, Langmuir **19**, 7977 (2003).
[12] A. I. Skoulidas and D. S. Sholl, J. Phys. Chem. B **105**, 3151 (2001).
[13] M. E. Davis, Nature (London) **417**, 813 (2002).
[14] C. Tunca and D. M. Ford, Chem. Eng. Sci. **58**, 3373 (2003).
[15] P. K. Ghorai and S. Yashonath, J. Chem. Phys. **120**, 5315 (2004).
[16] R. L. June, A. T. Bell, and D. N. Theodorou, J. Phys. Chem. **95**, 8866 (1991).
[17] E. Beerdsen, B. Smit, and D. Dubbeldam, Phys. Rev. Lett. **93**, 248301 (2004).
[18] D. Dubbeldam, E. Beerdsen, T. J. H. Vlugt, and B. Smit, J. Chem. Phys. **122**, 224712 (2005).
[19] E. Beerdsen, D. Dubbeldam, and B. Smit, Phys. Rev. Lett. **95**, 164505 (2005).
[20] A. I. Skoulidas, D. M. Ackerman, J. K. Johnson, and D. S. Sholl, Phys. Rev. Lett. **89**, 185901 (2002).
[21] S. S. Chong, H. Jobic, M. Plazanet, and D. S. Sholl, Chem. Phys. Lett. **408**, 157 (2005).